Minimal Model of Cellular Symmetry Breaking

Alexander Mietke,[1,2,3,4] V. Jemseena,[5] K. Vijay Kumar,[5] Ivo F. Sbalzarini,[2,4,3,6] and Frank Jülicher[1,3,6,*]
[1]Max Planck Institute for the Physics of Complex Systems, 01187 Dresden, Germany
[2]Chair of Scientific Computing for Systems Biology, Faculty of Computer Science, TU Dresden, 01187 Dresden, Germany
[3]Center for Systems Biology Dresden, 01307 Dresden, Germany
[4]Max Planck Institute of Molecular Cell Biology and Genetics, 01307 Dresden, Germany
[5]International Centre for Theoretical Sciences, Tata Institute of Fundamental Research, 560 089 Bengaluru, India
[6]Cluster of Excellence Physics of Life, TU Dresden, 01307 Dresden, Germany

(Received 20 May 2019; published 28 October 2019)

The cell cortex, a thin film of active material assembled below the cell membrane, plays a key role in cellular symmetry-breaking processes such as cell polarity establishment and cell division. Here, we present a minimal model of the self-organization of the cell cortex that is based on a hydrodynamic theory of curved active surfaces. Active stresses on this surface are regulated by a diffusing molecular species. We show that coupling of the active surface to a passive bulk fluid enables spontaneous polarization and the formation of a contractile ring on the surface via mechanochemical instabilities. We discuss the role of external fields in guiding such pattern formation. Our work reveals that key features of cellular symmetry breaking and cell division can emerge in a minimal model via general dynamic instabilities.

DOI: 10.1103/PhysRevLett.123.188101

The cortex of animal cells is a dynamically cross-linked polymer network located beneath the cell membrane [1]. It is involved in many important cellular symmetry-breaking events, such as the establishment of cell polarity [2,3] and cell division [4]. These processes typically involve cortical flows and cell shape changes, such that the cortex has to interact with material that surrounds it. Towards the inside of the cell, it is in contact with the cytoplasm, a crowded viscous fluid. By manipulating the cytoplasm mechanically, it has been shown that cytoplasmic flows can directly affect the dynamics of the cortex and the distribution of proteins within it [5]. The reverse scenario, in which active cortical flows set the cytoplasmic fluid into motion, has also been observed [6]. This suggests that the cytoplasmic fluid is coupled to the dynamics of the cell cortex and vice versa.

The cell cortex has been successfully described as a thin active fluid film [7]. Many aspects of the cortex' emergent dynamics can be accounted for by considering its generic mechanochemical organization [8]: The concentration of a diffusible chemical species regulates the amplitude of active stress, but also changes dynamically due to advection of the stress regulator by material flows. Spontaneous pattern formation in such self-organized active fluids has been studied on fixed domains with and without substrate friction [8–14] and on deforming surfaces in an environment with a homogeneous pressure [15].

In this Letter, we study a minimal model for the self-organization of an active surface that encloses a passive viscous fluid. A diffusing molecular species that regulates active tension on the surface provides a mechanochemical feedback. We show that the coupling of the surface to the enclosed fluid gives rise to a hydrodynamic screening length that guides mechanochemical instabilities to generate well-defined patterns on the surface. These patterns can govern shape changes and they can be oriented by external inhomogeneous signaling cues, which captures key features of symmetry-breaking events during important cellular processes.

We base our work on a simple hydrodynamic theory of a thin active fluid layer on a closed surface geometry [15]. The surface Γ is represented by a parametrization of surface position vectors $\mathbf{X}(s^1, s^2)$ with two generalized coordinates s^1, s^2. Tangent vectors and unit surface normal are given by $\mathbf{e}_i = \partial_i \mathbf{X}$ $(\partial_i = \partial/\partial s^i)$ and $\mathbf{n} = \mathbf{e}_1 \times \mathbf{e}_2/|\mathbf{e}_1 \times \mathbf{e}_2|$, respectively. Furthermore, we define the metric tensor $g_{ij} = \mathbf{e}_i \cdot \mathbf{e}_j$, the Levi-Civita tensor $\epsilon_{ij} = \mathbf{n} \cdot (\mathbf{e}_i \times \mathbf{e}_j)$, and the curvature tensor $C_{ij} = -\mathbf{n} \cdot \partial_i \partial_j \mathbf{X}$.

The force and torque balance on the surface read [16]

$$\nabla_i \mathbf{t}^i = -\mathbf{f}^{\mathrm{ext}}, \tag{1}$$

$$\nabla_i \mathbf{m}^i = \mathbf{t}^i \times \mathbf{e}_i. \tag{2}$$

Here, we have introduced the surface stress $\mathbf{t}_i = t_{ij}\mathbf{e}^j + t^i_n \mathbf{n}$, the surface moment $\mathbf{m}_i = m_{ij}\mathbf{e}^j + m^i_n \mathbf{n}$, and ∇_i denotes the covariant derivative. The external force per unit area is denoted $\mathbf{f}^{\mathrm{ext}} = f^{\mathrm{ext}}_i \mathbf{e}^i + f^{\mathrm{ext}}_n \mathbf{n}$. We do not include inertial forces and external torques. For simplicity, we do not consider deviatoric contributions to the moments. The tension and moment tensors in the surface can then be

written as $t_{ij} = t^e_{ij} + t^d_{ij}$, $m_{ij} = m^e_{ij}$, $t^i_n = t^{i,e}_n + t^{i,d}_n$, and $m^i_n = m^{i,e}_n$, where the superscripts e and d refer to equilibrium and deviatoric contributions, respectively.

Equilibrium contributions can be obtained by considering a passive membrane with bending rigidity κ, spontaneous curvature C_0, and passive surface tension γ as described by the Helfrich energy of a fluid membrane [15,17]. In this case [18]:

$$t^e_{ij} = \gamma g_{ij} + \kappa(C^k_k - 2C_0)[(C^k_k - 2C_0)g_{ij} - 2C_{ij}], \tag{3}$$

$$m^e_{ij} = 2\kappa(C^k_k - 2C_0)\epsilon_{ij}. \tag{4}$$

For the deviatoric part of the tension tensor, we consider contributions from an isotropic active fluid film. In-plane material flows $\mathbf{v}_\parallel = v^i\mathbf{e}_i$ and surface deformations $\mathbf{v}_\perp = v_n\mathbf{n}$ contribute to the center-of-mass velocity $\mathbf{v} = \mathbf{v}_\parallel + \mathbf{v}_\perp$ of the active fluid film. The deviatoric tension tensor is given by [15,18]

$$t^d_{ij} = 2\eta_s\left(v_{ij} - \frac{1}{2}v^k_k g_{ij}\right) + \eta_b v^k_k g_{ij} + \xi_{ij}. \tag{5}$$

Here, η_s and η_b denote shear and bulk viscosity of the two-dimensional material, respectively, and ξ_{ij} denotes an active tension. The strain rate tensor $v_{ij} = (\nabla_i v_j + \nabla_j v_i)/2 + C_{ij}v_n$ captures the shear rate and area expansion of the thin material.

With Eqs. (3) and (4), the torque balance Eq. (2) implies $m^{i,e}_n = 0$, $t^{i,d}_n = 0$ and $t^{i,e}_n = \epsilon^i_j \nabla_k m^{kj,e}$, and we can express the force balance Eq. (1) as

$$\nabla_i t^{i,d}_j = -f^{\mathrm{ext}}_j, \tag{6}$$

$$C^{ij}t^d_{ij} + f^e_n = f^{\mathrm{ext}}_n. \tag{7}$$

Here, we have defined $f^e_n = C^{ij}t^e_{ij} - \nabla_i t^{i,e}_n$ as the normal force exerted by a passive membrane [19,20]. With the deviatoric tension tensor t^d_{ij} from Eq. (5), Eqs. (6) and (7) yield the hydrodynamic equations for the tangential and normal flow velocity, $\mathbf{v}_\parallel$ and $\mathbf{v}_\perp$, respectively.

The active surface encloses a passive bulk fluid. We describe the latter as an incompressible Stokes fluid ($\nabla \cdot \mathbf{u} = 0$) obeying the force balance

$$\eta\Delta\mathbf{u} = \nabla p, \tag{8}$$

where $\mathbf{u}$ denotes the passive flow field, η is the shear viscosity, and p denotes the hydrostatic pressure. To solve Eq. (8), we impose no-slip and impermeability boundary conditions at the surface:

$$\mathbf{e}_i \cdot \mathbf{u}|_\Gamma = v_i, \tag{9}$$

$$\mathbf{n} \cdot \mathbf{u}|_\Gamma = v_n. \tag{10}$$

The forces $\mathbf{f}^{\mathrm{ext}}$ in Eqs. (6) and (7) result from viscous shear stresses that the passive fluid exerts on the surface. They are given by $\mathbf{f}^{\mathrm{ext}} = -\mathbf{n}\cdot\boldsymbol{\sigma}|_\Gamma$, where $\boldsymbol{\sigma} = \eta(\nabla\mathbf{u} + \nabla\mathbf{u}^T) - p\mathbb{I}$ is the stress tensor of the enclosed fluid.

The equations for the active surface and the bulk fluid are combined with an advection-diffusion equation for stress regulator molecules of area concentration c on the surface [18]:

$$\partial_t c + \nabla_i(cv^i) + C^k_k v_n c - D\Delta_\Gamma c = J_n. \tag{11}$$

Here, $\Delta_\Gamma = \nabla_i\nabla^i$ denotes the Laplace-Beltrami operator, D is a diffusion coefficient, and J_n describes the exchange of molecules between the thin film and the enclosed fluid. It is given by

$$J_n = k_{\mathrm{on}}\bar{c}|_\Gamma - k_{\mathrm{off}}c, \tag{12}$$

where k_{on} and k_{off} denote rates for the recruitment of the stress regulator to and detachment from the surface, respectively. $\bar{c}$ is the volume concentration of molecules in the enclosed bulk fluid. For simplicity, we consider the case where the diffusion of the stress regulator in the enclosed fluid is fast compared to its exchange with the thin film. Then, the concentration $\bar{c}$ is homogeneous with $d\bar{c}/dt = -V^{-1}\oint_\Gamma dA J_n$, where V is the volume of the enclosed bulk fluid.

Finally, the system is completed by a mechanochemical feedback [15]: The active tension ξ_{ij} in Eq. (5) depends on the local surface concentration c of the stress regulator molecules. We consider an active tension $\xi_{ij} = \xi f(c)g_{ij}$ that is isotropic within the surface, and the contractility ξ is modulated by a function $f(c)$ with $\partial_c f(c) > 0$ [8]. Because of the mechanical coupling between the thin film and the enclosed fluid, given in Eqs. (9) and (10), self-organized surface flows and deformations generated by active tension set the passive bulk fluid into motion.

Together, Eqs. (6), (7), (8), and (11) represent a minimal model for cortical flows that are coupled to the cellular cytoplasm [5]. This model has a simple stationary state in which the surface is given by a sphere of radius R_0, the surface concentration is homogeneous ($c = c_0$), and no flows exist ($\mathbf{v} = 0, \mathbf{u} = 0$). Two important timescales in this system are the timescale $\tau_c = \eta_b/\xi$ describing the advection-driven accumulation of stress regulator, and the diffusion timescale $\tau_D = R_0^2/D$. Then, $\mathrm{Pe} = \tau_D/\tau_c = \xi R_0^2/(D\eta_b)$ can be identified as Péclet number characterizing the activity in the system [8,11].

We now discuss the linear stability of the homogeneous stationary state in which the active surface is given by a sphere. Using spherical harmonics $Y_{lm}(\theta,\varphi)$ ($l = 0, 1, \ldots, \infty$; $m = -l, \ldots, l$), where θ and φ denote polar angle and azimuthal, respectively, as well as vector spherical

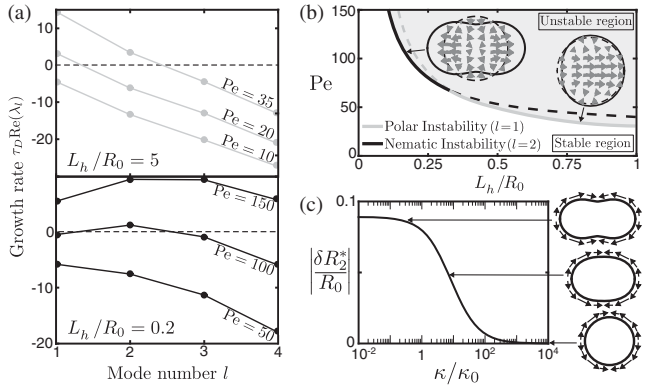

FIG. 1. (a) Eigenmode growth rates $\tau_D \mathrm{Re}(\lambda_l)$ as a function of mode number l for different Péclet numbers for larger (top) and smaller (bottom) hydrodynamic length $L_h = \eta_s/\eta$. Lines serve as a guide to the eye. (b) Linear stability diagram. The mode $l = 1$ ($l = 2$) becomes unstable first when moving across the gray (black) curve [Eq. (13)]. Insets visualize unstable modes: Arrows depict bulk flows, outlines indicate perturbed shapes (large perturbation amplitude for visualization). The stability diagram is independent of bending rigidity κ, spontaneous curvature C_0, and surface tension γ. (c) Contributions of deformations δR^*_{lm} to a critical eigenmode $\boldsymbol{\delta}^*_{lm} = (\delta R^*_{lm}/R_0, \delta c^*_{lm}/c_0)^T$ at $\mathrm{Pe} = \mathrm{Pe}^*_l$ as a function of κ [20], shown here for $l = 2$, $m = 0$ ($\kappa_0 = R_0^2 \eta_b/\tau_D$). Parameters: $\kappa = 0$ (a), $C_0 = 0$, $k_{\mathrm{off}}\tau_D = 10$, $\nu = 1$, and $c_0 \partial_c f(c_0) = 1$.

harmonics $\boldsymbol{\Psi}^{(lm)} = R_0 \nabla_\Gamma Y_{lm}$ and $\boldsymbol{\Phi}^{(lm)} = \hat{\mathbf{r}} \times \boldsymbol{\Psi}^{(lm)}$, we express shape, concentration, and flow perturbations as $\delta R = \sum_{l,m} \delta R_{lm} Y_{lm}$, $\delta c = \sum_{l,m} \delta c_{lm} Y_{lm}$, and $\delta \mathbf{v}_\parallel = \sum_{l,m} (\delta v^{(1)}_{lm} \boldsymbol{\Psi}^{(lm)} + \delta v^{(2)}_{lm} \boldsymbol{\Phi}^{(lm)})$ [15].

We expand Eqs. (6), (7), (8), and (11) to linear order in these fields [20,27]. After eliminating the flow fields, the dynamics of each mode has the form $(d/dt)(\delta R_{lm}, \delta c_{lm})^T = \mathcal{J}_l (\delta R_{lm}, \delta c_{lm})^T$, where $\mathcal{J}_l$ is the Jacobian. Its eigenvalues λ_l are the growth rates of eigenmodes $\boldsymbol{\delta}_{lm} = (\delta R_{lm}, \delta c_{lm})^T$. For a vanishing or small Péclet number Pe, we have $\mathrm{Re}(\lambda_l) < 0$, and the steady state is stable [Fig. 1(a)]. For an increasing Péclet number and independently of the azimuthal mode number m, modes with $l \geq 1$ become unstable at $\mathrm{Pe} = \mathrm{Pe}^*_l$, where

$$\mathrm{Pe}^*_l = \frac{1}{c_0 \partial_c f(c_0)} \left(1 + \frac{\tau_D k_{\mathrm{off}}}{l(l+1)}\right) \times \left[l(l+1) + \nu \left((l-1)(l+2) + (1+2l)\frac{R_0}{L_h}\right)\right] \tag{13}$$

is the critical Péclet number for a mode l [20]. Here, we have defined the surface viscosity ratio $\nu = \eta_s/\eta_b$, as well as the hydrodynamic length $L_h = \eta_s/\eta$. Remarkably, Pe^*_l is independent of bending rigidity κ, spontaneous curvature C_0, and surface tension γ. Therefore, Eq. (13) equals the expression found in the limit of large κ, where the surface becomes a rigid sphere [20].

We now discuss Eq. (13) and key properties of the unstable modes in more detail. For small viscosities of the passive fluid $\eta \lesssim \eta_s/R_0$, the mode $l = 1$ becomes unstable first for increasing Péclet number. The instability of $l = 1$ corresponds to a vectorial (polar) symmetry breaking. In the limit of large L_h the viscosity of the surrounding passive fluid can be neglected and we recover the result reported in [15]. Interestingly, for finite turnover $k_{\mathrm{off}} > 0$ the nematic mode $l = 2$ can become unstable, while $l = 1$ is still stable [Fig. 1(a), bottom]. It follows from Eq. (13) that this can only occur for a small hydrodynamic length, $L_h \lesssim R_0$, corresponding to a regime where the stresses exerted by the enclosed passive fluid are significant. This implies that the hydrodynamic screening length L_h plays a crucial role in selecting a specific wavelength for patterns on the surface. For finite surface tension γ and bending rigidity κ, the eigenmode associated with this instability is given by an ingression of the spherical surface along a ring of high stress regulator concentration. Critical eigenmodes $\boldsymbol{\delta}^*_{lm}$ and a stability diagram of the spherical state as a function of the Péclet number and hydrodynamic length are shown in Fig. 1(b). The homogeneous sphere is unstable in the gray shaded region. The polar ($l = 1$) and nematic ($l = 2$) instabilities, depicted by the gray and black curves, respectively, are given by Eq. (13). For $l \geq 2$, critical eigenmodes depend on the bending rigidity κ and the surface tension γ. In particular, contributions from deformations $\delta R^*_{lm}/R_0$ to the eigenmode vanish for large surface tension or bending rigidity [Fig. 1(c)] [20].

To study the nonlinear dynamics beyond the discussed instabilities, we use numerical methods [20]. For simplicity, we consider the limit of large bending rigidity κ, where the surface is not deformed. We first discuss the case $L_h/R_0 = 5$, where the polar mode becomes unstable first. Using a small random concentration perturbation as the initial condition, the instability of $l = 1$ leads to an axisymmetric steady-state pattern exhibiting a single patch of high stress regulator concentration [Figs. 1(a)–1(c)]. A cross section that contains the polar axis defined by this pattern reveals a hydrodynamic flow field with a backflow along the symmetry axis, driven by the active surface flows that maintain the pattern. For $L_h/R_0 = 0.2$ the mode $l = 2$ can become unstable first for increasing Péclet number [Fig. 1(b)]. In this case, a random perturbation leads to the formation of a ring of high stress regulator concentration along the equator [Figs. 2(d)–2(f)]. This ring corresponds to a circumferential contractile ring of active tension that can constrict a deformable sphere. In this state, the passive fluid flow exhibits two toroidal vortex tubes, stacked orthogonally to the nematic axis and rotating in opposite directions. Further away from the instability threshold, numerical calculations reveal the existence of oscillatory patterns in certain regimes [20].

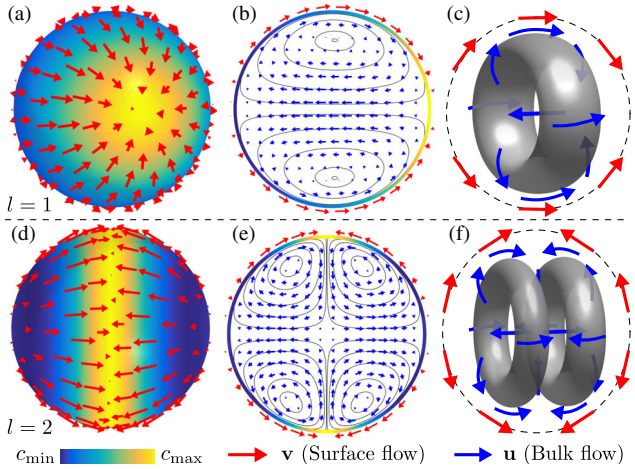

FIG. 2. (a) An instability of the mode $l = 1$ leads to a surface pattern with polar symmetry. (b) Corresponding cross-sectional view parallel to the axis defined by the surface patterns. Black lines depict streamlines. (c) Schematic representation of the global flow topology. Gray tori depict vortex rings, blue arrows indicate their direction of rotation. (d)–(f) In regimes where $l = 2$ is the only unstable mode, a contractile ring with nematic symmetry forms. Parameters: $\mathrm{Pe} = 20$, $L_h/R_0 = 5$ $(l = 1)$; $\mathrm{Pe} = 100$, $L_h/R_0 = 0.2$ $(l = 2)$; $k\tau_D = 10$, $\nu = 1$, $\kappa \to \infty$ $(l = 1, 2)$. Active tension is regulated by $f(c) = 2c^2/(c_0^2 + c^2)$, such that $c_0 \partial_c f(c_0) = 1$.

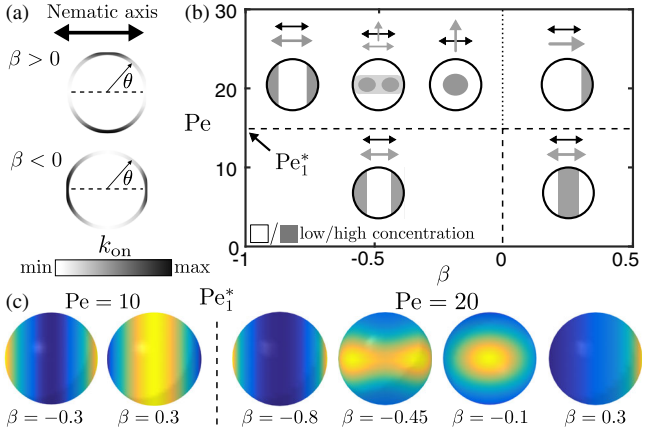

FIG. 3. (a) Cross-sectional views on recruitment rate $k_{\mathrm{on}}(\theta)$ [Eq. (14)]. β determines the amplitude and sign of the nematic cue. (b) Schematic representation of surface patterns and their orientation for varying Péclet number Pe and strength of the nematic cue β in a regime where $l = 1$ becomes unstable first at $\mathrm{Pe} = \mathrm{Pe}_1^*$ if $\beta = 0$ (dotted line). Gray arrows depict the orientation and symmetry axes defined by the surface patterns. For $\mathrm{Pe} < \mathrm{Pe}_1^*$ and $\beta \neq 0$, steady-state surface patterns are dictated by $k_{\mathrm{on}}(\theta)$. For $\mathrm{Pe} > \mathrm{Pe}_1^*$ and $\beta \neq 0$, spontaneously forming patterns on the surface interact with the nematic cue. (c) Representative steady-state concentration patterns obtained from numerical solutions. Qualitative color code as in Figs. 1(a) and 1(d). Parameters: $L_h/R_0 = 5$, $k_{\mathrm{off}}\tau_D = 10$, and $\nu = 1$.

The nematic instability provides a minimal model for the self-organized formation of a contractile ring that can drive constriction during cell division. In our model, the axis characterizing the contractile ring is defined by a spontaneous symmetry-breaking event. This is different from biological systems, where the contractile ring, and hence the division axis, are oriented along the mitotic spindle via biasing signaling cues [28,29]. Also cell polarization, a process that is key to asymmetric cell divisions, depends on the coordination between spindle orientation and the biochemical organization of the cellular cortex [30]. In order to include such a symmetry-breaking bias in our model, we generalize the expression for the flux J_n given in Eq. (12) and consider an angle dependent recruitment rate $k_{\mathrm{on}}(\theta)$ of stress regulator on the surface, described by

$$k_{\mathrm{on}}(\theta) = k_{\mathrm{on}}^{(0)}[1 + \beta(1 - 3\cos^2\theta)]. \tag{14}$$

The coefficient β determines the strength and sign of the nematic bias. It varies in the interval $[-1, 1/2]$, such that $k_{\mathrm{on}}(\theta) \geq 0$. For $\beta > 0$ $(\beta < 0)$, there is a recruitment of stress regulator predominantly to the equator region near $\theta = \pi/2$ (to the opposing poles at $\theta = 0, \pi$) [Fig. 3(a)].

We first consider the effects of the nematic cue on the self-organized pattern formation in the regime where the polar mode $l = 1$ becomes unstable first for the increasing Péclet number (Fig. 3). For $\mathrm{Pe} < \mathrm{Pe}_1^*$, the homogeneous state is stable in the absence of the cue $(\beta = 0)$, while $\beta \neq 0$ leads to the formation of a concentration pattern with the nematic symmetry dictated by $k_{\mathrm{on}}(\theta)$. For $\mathrm{Pe} > \mathrm{Pe}_1^*$, the polar instability in the presence of a nematic cue leads to more complex surface patterns that combine polar and nematic features [Fig. 3(b)]. For $\beta > 0$ a polar surface pattern forms, whose axis is oriented parallel to the axis of the nematic cue. For $\beta < 0$, we can qualitatively distinguish three regimes. If $|\beta|$ is small, a single contractile patch forms, defining a polar axis that is oriented orthogonal to the nematic cue axis. If $|\beta|$ is increased, two local concentration maxima appear. If $|\beta|$ is increased further, the nematic cue dominates, leading to a pattern with two patches of stress regulator at opposing poles aligned by the cue. Figure 3(c) shows examples of steady-state concentration patterns for these different cases.

We also found that in the case of an instability with nematic symmetry $(l = 2)$, a cue with $\beta > 0$ ensures that the nematic axis of the emerging contractile rings is reliably oriented parallel to the axis of the nematic cue. This captures the effect of a mitotic spindle with nematic symmetry orienting the contractile ring along the division axis.

In this Letter, we have studied the mechanochemical self-organization of active fluid surfaces with spherical geometry. We have shown that the viscous forces exerted by a passive fluid on an enclosing active fluid film can control the formation of patterns with different symmetries.

We have found that the active surface can undergo spontaneous symmetry-breaking instabilities toward

patterns of concentration, flows, and deformations with polar or nematic symmetries, depending on the ratio L_h/R_0 of hydrodynamic screening length to sphere radius. For large ratios, polar patterns emerge, corresponding to the mode $l = 1$, while patterns can be nematic, corresponding to $l = 2$, for smaller ratios L_h/R_0. When decreasing the ratio L_h/R_0 even further, stationary patterns corresponding to higher harmonic modes $l > 2$ can emerge. These have a polar symmetry for odd l and a nematic symmetry if l is even [20].

For simplicity, we considered here an isotropic active tension. In general, an anisotropic contribution to the active tension of the form $\xi'_{ij} = \xi' f(c) C_{ij}$ exists. When taking such anisotropies in active tension into account, the results presented here do not change qualitatively, but the critical Péclet number is altered for $l > 1$ [20].

The emergence of mechanochemical patterns presented in this work generalizes the one-dimensional contractile instabilities described in [8] to curved surfaces. Instabilities on the surface of a sphere discussed here capture key features of important cellular processes. The emergence of polar patterns resembles the establishment of cell polarity by active processes in the cell cortex [31–33]. The emergence of an equatorial ring of high contractility provides a minimal model for the formation of contractile rings that play a key role during cell division [1,4]. Symmetry-breaking instabilities can be biased by external chemical cues. In particular, we found the axis of a contractile ring can be reliably aligned with the axis of a nematic cue, similar to the alignment of a contractile ring with the mitotic spindle axis during cell division [28,29].

Considering a passive fluid outside of the active surface also leads to the formation of patterns via dynamic instabilities. During the polar instability, a net flow outside the surface is generated. Driven by active surface flows, the sphere will therefore move relative to the laboratory frame [20], corresponding to a swimmer that exhibits spontaneous self-propulsion. For the case of vanishing surface viscosity $\eta_b = \eta_s = 0$, this scenario is similar to swimmers driven by Marangoni flows [34,35].

Our minimal model captures general features of the contractile actomyosin cortex of cells and its mechanical interactions with the cytoplasm. To account for more complex features of the cell cortex [1], it could be extended, for example, by including multicomponent descriptions of the biochemical processes. Finally, the instabilities and surface patterns discussed here could be studied experimentally using *in vitro* actomyosin systems reconstituted in vesicles or in droplets [36–38].

A. M. acknowledges funding from an ELBE Ph.D. fellowship. This work was financially supported by the German Federal Ministry of Research and Education, Grant No. 031L0044 and by the Deutsche Forschungsgemeinschaft (DFG, German Research Foundation) under Germany's Excellence Strategy EXC-2068-390729961, Cluster of Excellence Physics of Life of TU Dresden. V. J. and K. V. K. acknowledge support from the Max-Planck partner group at the International Centre for Theoretical Sciences (ICTS) of the Tata Institute of Fundamental Research in India. K. V. K. is supported by the Department of Biotechnology, India, through a Ramalingaswami reentry fellowship.

*Corresponding author.
julicher@pks.mpg.de

[1] G. Salbreux, G. Charras, and E. Paluch, Trends Cell Biol. **22**, 536 (2012).
[2] N. W. Goehring, P. K. Trong, J. S. Bois, D. Chowdhury, E. M. Nicola, A. A. Hyman, and S. W. Grill, Science **334**, 1137 (2011).
[3] A. C. Callan-Jones, V. Ruprecht, S. Wieser, C. P. Heisenberg, and R. Voituriez, Phys. Rev. Lett. **116**, 028102 (2016).
[4] J. White and G. Borisy, J. Theor. Biol. **101**, 289 (1983).
[5] M. Mittasch, P. Gross, M. Nestler, A. W. Fritsch, C. Iserman, M. Kar, M. Munder, A. Voigt, S. Alberti, S. W. Grill, and M. Kreysing, Nat. Cell Biol. **20**, 344 (2018).
[6] S. N. Hird and J. G. White, J. Cell Biol. **121**, 1343 (1993).
[7] M. Mayer, M. Depken, J. S. Bois, F. Jülicher, and S. W. Grill, Nature (London) **467**, 617 (2010).
[8] J. S. Bois, F. Jülicher, and S. W. Grill, Phys. Rev. Lett. **106**, 028103 (2011).
[9] S. Banerjee and M. C. Marchetti, Soft Matter **7**, 463 (2011).
[10] Niladri Sarkar and Abhik Basu, Eur. Phys. J. E **36**, 86 (2013).
[11] K. V. Kumar, J. S. Bois, F. Jülicher, and S. W. Grill, Phys. Rev. Lett. **112**, 208101 (2014).
[12] T. Moore, S. K. Wu, M. Michael, A. S. Yap, G. A. Gomez, and Z. Neufeld, Biophys. J. **107**, 2652 (2014).
[13] I. M. Sehring, P. Recho, E. Denker, M. Kourakis, B. Mathiesen, E. Hannezo, B. Dong, and D. Jiang, eLife **4**, 1 (2015).
[14] C. A. Weber, C. H. Rycroft, and L. Mahadevan, Phys. Rev. Lett. **120**, 248003 (2018).
[15] A. Mietke, F. Jülicher, and I. F. Sbalzarini, Proc. Natl. Acad. Sci. U.S.A. **116**, 29 (2019).
[16] H. Berthoumieux, J.-L. Maître, C.-P. Heisenberg, E. K. Paluch, F. Jülicher, and G. Salbreux, New J. Phys. **16**, 065005 (2014).
[17] W. Helfrich, Z. Naturforsch. C **28**, 693 (1973).
[18] G. Salbreux and F. Jülicher, Phys. Rev. E **96**, 032404 (2017).
[19] O.-Y. Zhong-can and W. Helfrich, Phys. Rev. A **39**, 5280 (1989).
[20] See Supplemental Material at http://link.aps.org/supplemental/10.1103/PhysRevLett.123.188101 for detailed derivations and information about the numerical methods, which includes Refs. [21–26].
[21] R. Capovilla and J. Guven, J. Phys. A **35**, 6233 (2002).
[22] V. D. Sandberg, J. Math. Phys. (N.Y.) **19**, 2441 (1978).
[23] J. A. Gaunt, Phil. Trans. R. Soc. A **228**, 151 (1929).
[24] N. Sneeuw, Geophys. J. Int. **118**, 707 (1994).
[25] J. R. Dormand and P. J. Prince, J. Comput. Appl. Math. **6**, 19 (1980).
[26] Matlab 2015b, The MathWorks, Natick, MA, USA.

[27] R. Seyboldt and F. Jülicher, New J. Phys. **20**, 105010 (2018).
[28] M. Théry, A. Jiménez-Dalmaroni, V. Racine, M. Bornens, and F. Jülicher, Nature (London) **447**, 493 (2007).
[29] N. T. L. Rodrigues, S. Lekomtsev, S. Jananji, J. Kriston-Vizi, G. R. X. Hickson, and B. Baum, Nature (London) **524**, 489 (2015).
[30] X. Morin and Y. Bellaïche, Dev. Cell **21**, 102 (2011).
[31] P. Gross, K. V. Kumar, N. W. Goehring, J. S. Bois, C. Hoege, F. Jülicher, and S. W. Grill, Nat. Phys. **15**, 293 (2019).
[32] H. A. Benink, C. A. Mandato, and W. M. Bement, Mol. Biol. Cell **11**, 2553 (2000).
[33] K. Yi, J. R. Unruh, M. Deng, B. D. Slaughter, B. Rubinstein, and R. Li, Nat. Cell Biol. **13**, 1252 (2011).
[34] A. Zöttl and H. Stark, J. Phys. Condens. Matter **28**, 253001 (2016).
[35] C. A. Whitfield and R. J. Hawkins, New J. Phys. **18**, 123016 (2016).
[36] M. Murrell, L.-L. Pontani, K. Guevorkian, D. Cuvelier, P. Nassoy, and C. Sykes, Biophys. J. **100**, 1400 (2011).
[37] K. Carvalho, F.-C. Tsai, E. Lees, R. Voituriez, G. H. Koenderink, and C. Sykes, Proc. Natl. Acad. Sci. U.S.A. **110**, 16456 (2013).
[38] E. Abu Shah and K. Keren, eLife **3**, e01433 (2014).